

**Remote sensing of extra-equatorial planetary waves  
in the oceans**

***Paolo Cipollini, Graham D. Quartly, Peter G. Challenor, David  
Cromwell and Ian S. Robinson***

***Laboratory for Satellite Oceanography, Southampton  
Oceanography Centre, U. K.***

**A contribution to Manual of Remote Sensing**

**Revision 05/04/2004**

Corresponding author:

Dr. Paolo Cipollini

Room 254/30, Southampton Oceanography Centre

European Way, SO14 3ZH Southampton, United Kingdom

Ph. +44-23-80596404 fax: 80596400 e-mail: [cipo@soc.soton.ac.uk](mailto:cipo@soc.soton.ac.uk)

# Remote sensing of extra-equatorial planetary waves in the oceans

Waves in the ocean exist on a wide variety of spatial and temporal scales. A particularly interesting and important type is planetary waves, which are large-scale (hundreds to thousands of kilometres wavelength) perturbations of the ocean interior, with a surface signature of only a few centimetres amplitude. Their existence, due to the shape and rotation of the earth, was first predicted at the end of the 19th century, but nearly 100 years passed before it was realised that they were present throughout the ocean and could play a major role in maintaining and/or changing western boundary currents. The justification behind the study of these waves not only resides in their fascinating properties and in the fact that their detection has been a success story for marine remote sensing in recent years, but also, and more significantly, in their paramount importance for ocean circulation and climate, as will be clarified in the following.

The analysis presented in this section is restricted to extra-equatorial planetary waves because in the equatorial band the ocean dynamics results in propagating phenomena with generally longer spatial scales and faster speeds than their counterparts at mid-latitude (see below for further details). These equatorial waves are in some cases difficult to observe in satellite data (as the data may lack the necessary time resolution) or may require different analytical techniques for their identification, and will not be dealt with here.

## 1. Theory and properties of planetary waves

The physical principle underlying planetary waves, both in the ocean and the atmosphere, is the conservation of potential vorticity when a parcel of fluid (water or air) on the surface of a rotating sphere is displaced in the N-S direction (called the *latitudinal* or *meridional* direction, as opposed to the E-W or *zonal* direction), thus being subject to a variation of the Coriolis parameter. For instance, when a small region of the ocean responds to a change in conditions (e.g. a change in current direction or additional wind stress) the system is disturbed locally. If the response has involved a latitudinal displacement of water, then potential vorticity (a

quantity akin to the parcel's angular momentum about the Earth's axis) provides a restoring force. Since the restoring force is proportional to the displacement the result is a sinusoidal signal, an intriguing property of which is that the propagation is westward, although the displacements are meridional (see Fig. 1).

Hough (1897) was the first to formulate the equations for planetary wave motion on a rotating sphere and discussed the solutions in spherical coordinates. Rossby et al. (1939) and Rossby (1940) approximated the problem into Cartesian coordinates on the so-called ‘ $\beta$ -plane’. They did this by assuming that the Coriolis parameter  $f = 2\Omega\sin\theta$ , where  $\Omega$  is the rotation rate of the earth ( $7.29 \times 10^{-5}$  rad/s) and  $\theta$  is the latitude, varies linearly with latitude, and could thus be written as  $f = f_0 + \beta y$  where  $y$  is the meridional (north-south) coordinate and  $\beta = \partial f / \partial y$ . Those papers identified patterns of planetary waves in the atmosphere. In virtue of Carl-Gustav Rossby’s essential contribution to the subject, planetary waves are also widely known as Rossby waves. As stated in the introduction to this section, in the vicinity of the equator ( $f \approx 0$ ) the equations for large-scale motion have to be solved with different approximations from the extra-equatorial case, and the dynamics of planetary and gravity waves become inter-related (see for instance chapter 8.5 of Pedlosky (1987)). In the following, therefore, the discussion will be restricted to extra-equatorial Rossby waves outside the  $5^\circ\text{S}$ - $5^\circ\text{N}$  latitude band, but for the sake of brevity they will be referred to simply as planetary waves here.

The low-frequency propagating solutions of the planetary wave equations outside the equatorial band are classically obtained with a further linearization about a state of zero background flow. These solutions can be cast on a number of orthogonal vertical *modes* with different depth structures identified by a mode number  $n$ . The mode with  $n=0$  is depth-invariant and is called the *barotropic* mode. Modes with  $n>0$  are depth-varying and called the *baroclinic* modes (the complete terminology is ‘first baroclinic’ for  $n=1$ , ‘second baroclinic’ for  $n=2$ , and so on). The speed of the modes is given by the so-called dispersion relationship, i.e. the relationship linking frequency and wavenumber of the mode. For propagating solutions of the form  $\psi \sim \exp\{i \times (kx + ly - \omega_n t)\}$ , it turns out that the dispersion relation can be written as:

$$c_{nx} = \frac{\omega_n}{k} = -\frac{\beta}{k^2 + l^2 + \lambda_n^2} \quad (1)$$

This provides the westward zonal *phase speed*  $c_{nx}$  where  $n$  is the mode number,  $k$ ,  $l$  are the zonal (east-west) and meridional (north-south) wavenumbers,  $\omega_n$  is frequency and  $\lambda_n$  is a characteristic length scale in the oceans known as the *Rossby radius of deformation* for mode  $n$ . Equation (1) is a reasonable approximation throughout the deep ocean where friction effects and nonlinear advection are negligible. The Rossby radius  $\lambda_n$  depends on density stratification and on  $1/|f|$ . Updated global maps of  $\lambda_0$  and  $\lambda_1$  from historic hydrographic data can be found in Chelton et al. (1998);  $\lambda_1$  is typically a few tens of kilometres at mid-latitudes. The barotropic mode travels at many metres per second, traversing ocean basins in a matter of weeks, often too fast to be resolved by satellites, so this will not concern us. However, there is a great deal of interest in the much slower baroclinic modes, especially the first baroclinic mode, depicted in figure 1. The baroclinic modes travel at speeds of the order of 1-10 cm/s (the higher the mode number, the slower the speed) and can affect the western boundary currents, and thus have major repercussions on climate.

The minus sign on the right hand side of eq. (1) indicates that the zonal phase speed of planetary waves is always westward: this is a consequence of the direction of the Earth's rotation. The meridional speed of the waves is usually negligible, i.e. they tend to propagate westward or quasi-westward. Their wavelength is typically of hundreds or thousands of kilometres, so they can be considered 'long' with respect to the Rossby radius, that is  $k, l \ll 1/\lambda_n^2$ ; as a consequence,  $c_{nx} = -\beta\lambda_n^2$  and the waves can also be regarded as non-dispersive. The speed in that case varies with latitude approximately as  $\cos\theta/\sin^2\theta$  (see the solid line in the upper panel of figure 2). It can be demonstrated that in the long-wave approximation both the phase and *group* velocities (group velocity is the velocity at which pulses or "wave packets", made up of a range of different spectral components, travel) are exactly westward, and that there exists a polewards latitude limit (called *turning latitude*) beyond which planetary wave solutions become evanescent, i.e. no propagation exists (see Gill (1982), pp. 440-443 for further details). For example, annual cycle baroclinic waves can only exist for latitudes less than about 45°.

The importance attached to baroclinic planetary waves in modern oceanography stems from multiple reasons: not only can they be regarded as the key response of the oceans to large-scale changes in atmospheric forcing, and as the only means (other than boundary waves) by which information is transferred from the eastern ocean boundaries to the west (e.g. Gill, 1982), but they also interact with the strong western boundary currents such as the Kuroshio

Current and the Gulf Stream, and, indeed, maintain these currents. Under particular circumstances, planetary waves can even be responsible for disturbing the position of the western boundary currents. For instance, Jacobs et al. (1994) present evidence for the existence of an extra-tropical Rossby wave in the North Pacific, generated by the El Niño event of 1982-83, and suggest that after a decade's delay this wave induced a shifting of the Kuroshio Current in the north-west Pacific. This shift may have affected the climate of North America, and been responsible for the dramatic meteorological events in North America in 1993, such as the Mississippi flooding (McPhaden, 1994). In short, as well as being one of the ways the ocean itself *responds* to climate events, Rossby waves may also delay the effects of these events and control the dynamics of climate change and weather variability.

## **2. Altimetric observations of planetary waves**

### ***2.1 Historical notes***

The important properties outlined in §1 have stimulated research on the occurrence, distribution and generation mechanism of planetary waves in the oceans, as well as on their properties, first and foremost their speed. But for many decades oceanographers found themselves in the uncomfortable position of having an accepted theory for the phenomenon but very scarce observational evidence for it, due to the inherent difficulties in measuring planetary waves *in situ*, mainly because of the sheer difference in the wave horizontal and vertical scales. Despite those difficulties, early proof of the occurrence of baroclinic planetary waves in the ocean, namely variations in the depths of subsurface isotherms, was reported by, amongst others, Emery and Magaard (1976) and White (1977). Over the next few years, a sizeable body of evidence was built up, demonstrating the existence of Rossby waves in the North Pacific ocean, in particular (see §3.4 of Fu and Chelton, 2001, for a full review of the *in situ* observations). These pioneering studies indeed confirmed the existence of planetary waves in the oceans, but due to the limitations of sampling could not provide the desired characterization of the wave distributions and properties.

In more recent years, satellite altimeters have given indisputable confirmation of the quasi-ubiquitous presence of planetary waves in the oceans. An earth-orbiting altimeter is in principle capable of detecting their surface signature as westward propagating features in maps of sea surface height anomalies (SSHAs), and this makes measurement of their

characteristics (speed, wavelength, period) possible. It should be kept in mind that the surface signature of the waves depends on integral properties of the whole water column; in the illustration of a first-mode baroclinic wave shown in figure 1 the surface mirrors (with amplitude reduced by about three orders of magnitude) the undulations of the thermocline (the thermocline, sited at the bottom of the surface mixed layer, is a region of relatively strong temperature and density change).

For the altimetric measurements of SSHA to be useful in practice, the following conditions need to occur:

- a) The accuracy of the SSHA field must be enough to detect signals of just a few cm, which is the typical planetary wave amplitude;
- b) The spatio-temporal sampling pattern of the altimeter and the length of the time series are appropriate to resolve the phenomenon;
- c) Other causes of SSHA variability can be identified and filtered out from the data. This in turn requires that the relevant phenomena have typical spatial and temporal scales distinguishable from those of planetary waves and that the sampling characteristics of the altimeter do not alias those signals in a way that they might be misinterpreted as planetary waves (see Parke et al. (1998) for a general discussion on aliasing problems in altimeter data).

Of the first two altimetric missions, GEOS-3 lacked the necessary accuracy (condition a) and SeaSat the time duration (b). The first direct altimetric observations of baroclinic planetary waves thus were in the Geosat dataset (for instance White et al, 1990; Jacobs et al., 1992, 1993; Le Traon and Minster, 1993; Tokmakian and Challenor, 1993). Unfortunately, Geosat suffered in respect to condition c): its 17-day repeat pattern meant that any residual  $M_2$  tidal signal (tide not completely removed from the SSHA data – see the relevant chapter) would be aliased at frequencies comparable with those of planetary waves, confusing the interpretation of the results. However these pioneering studies firmly established the use of tools such as the longitude/time plot and the relevant frequency/wavenumber diagram as the most natural approach to investigate planetary wave propagation in satellite data – what was clear at the time was that new spaceborne instruments were needed, with orbits designed to avoid the tidal aliasing problem.

The launch of TOPEX/POSEIDON (T/P) in 1992 marked the start of a new era in the observations of planetary waves from space. Its 10-day repeat orbit pattern was specifically selected to avoid tidal aliasing into frequencies of large-scale oceanic variability. Early T/P studies identified planetary waves in various regions of the world's oceans (Nerem et al, 1994, Wang and Koblinsky, 1995, 1996) but it was the global study of Chelton and Schlax (1996) which demonstrated the ubiquity of the waves and showed that at mid-latitude they tend to propagate faster than predicted by the linear theory (that is, faster than the speed given by eq. 1 in the  $l=0$  approximation, using atlases of  $\lambda_1$  based on historical hydrographic data). A number of theories have been proposed in the attempt to reduce the discrepancy in speed; the one yielding the most promising results to date is the extended theory by Killworth et al. (1997) which, by including the effects of the baroclinic background mean flow, more closely approaches the observed speed. Killworth et al.'s theory has been further extended or clarified by Dewar (1998), Liu (1999), de Szoeke and Chelton (1999), and Killworth and Blundell (1999, 2003a, 2003b). Figure 2, taken from Fu and Chelton, 2001, shows an updated version of the speeds measured by Chelton and Schlax (1996), as well as the ratios of the speeds to the prediction of the linear theory and the extended theory by Killworth et al. (1997). The discrepancy between the observed speed and the linear theory speeds is apparent in the upper and middle panel; the adoption of the extended theory greatly reduces this discrepancy as shown in the bottom panel (a residual underestimation of the speed remains at mid-latitudes in the southern hemisphere). A number of studies using altimeter data have contributed to map the characteristics of the waves, including Polito and Cornillon (1997) and the recent papers by Polito and Liu (2003), Fu (2004) and Osychny and Cornillon (2004).

## **2.2 Techniques**

This subsection discusses some processing techniques for the study of planetary waves in altimetric and other satellite data. In view of the wave's substantially east-west propagation, initially the focus will be on the techniques used to observe the zonal characteristics for mode  $n$  (zonal speed  $c_{nz}$ , zonal wavelength  $1/k$  and frequency  $\omega$ ). As said in §2.1, the usual approach for such an analysis is to build a particular kind of space-time diagram, called a longitude-time plot or Hovmöller diagram. This can be easily obtained by taking, for each time step, a section of data (SSHAs) at a given latitude and stacking all the sections from different cycles, as exemplified in figure 3 for 25°S in the Indian Ocean. The time step of the data in figure 3 is equal to an orbital cycle of the altimeter, that is 9.92 days for T/P. Planetary

waves appear clearly in the plot as diagonal alignments: positive anomalies ('crests') and negative anomalies ('troughs') that travel westward with time. Those in figure 3 have fairly constant speed, but variations are possible in some locations; those will be discussed later.

Although some of the characteristics of the propagating waves in a longitude/time plot can be approximately measured by eye (for instance, the speed is inversely proportional to the slope of the alignments and could be roughly estimated by fitting a ruler to the plot itself), more objective methods are needed. A number of two-dimensional data processing techniques lend themselves to this purpose. The two most common ones, that is the two-dimensional Fourier Transform (2D-FT) and Radon Transform (2D-RT), will be described in the following subsections. Both these transforms map the longitude/time plot onto a transformed space, that is the wavenumber/frequency (WF) space for the FT and a hybrid velocity/projected coordinate space for the RT.

## 2.2.1 Use of the Fourier Transform

In practice, the 2D-FT of longitude time plots is implemented with the Fast Fourier Transform algorithm (2D-FFT). It highlights the different spectral components of the plots, which appear as peaks in the transform or *spectrum* in the WF domain. The 2D-FT is a straightforward extension of the one-dimensional Fourier Transform (for more details on general Fourier transform theory and FFT see Brigham (1988)). For an image  $s(m\Delta x, n\Delta y)$  of  $M \times N$  pixels, where  $m, n$  are the pixel indices and  $\Delta x, \Delta y$  the resolutions (pixel dimensions) in the  $x$  and  $y$  directions, the 2D-FT is given by

$$S(f_x, f_y) = \Delta x \Delta y \sum_{m=1}^M \sum_{n=1}^N s(m\Delta x, n\Delta y) e^{-j2\pi(f_x \Delta x + f_y \Delta y)}$$

and in any practical implementation (including the 2D-FFT algorithm) it is computed on a discrete grid  $S(p\Delta f_x, q\Delta f_y)$ ,  $p = 1 \dots M$ ,  $q = 1 \dots N$  with frequency (or wavenumber) resolutions  $\Delta f_x = 1/(M\Delta x)$  and  $\Delta f_y = 1/(N\Delta y)$ .  $S$  is periodic in both the  $f_x$  and  $f_y$  directions, with periods  $1/\Delta x$  and  $1/\Delta y$ , and is generally complex, showing both the *amplitude* and *phase* of each spectral component. In the particular case where the initial plot has space (longitude)

along  $x$  and time along  $y$ , the transformed  $f_y$  axis corresponds to frequency proper (that is the inverse of time) and  $f_x$  to wavenumber (that is the inverse of space). Details on the 2D-FT and other transforms for image analysis can be found in Jain (1989).

The 2D-FFT has long been used for the processing of altimetric data in the literature (Le Traon and Minster, 1993, Tokmakian and Challenor, 1993); one of its advantages is that it allows the detection of the single components of the propagating signals, which stand out as peaks in the WF space and may correspond to the different baroclinic modes as suggested by Cipollini et al. (1997) at 34°N in the North Atlantic and also observed by Subrahmanyam et al. (1998) in the tropical Indian Ocean.

An example of application of the 2D-FFT is shown in figure 4. Figure 4a displays the longitude/time plot, at latitude 28°S, longitude 55°E to 75°E in the Indian Ocean from weekly, 1/3° SSHA data (data used for figures 4 to 7 are the DUACS merged T/P and ERS SSHAs produced by the CLS Space Oceanography Division) spanning the period from mid-October 1992 to early August 2002, for a total of 513 weeks. In the plot, the seasonal cycle has been removed or *filtered out* by subtracting from each row the mean value of that row (a more general 2D filtering technique will be briefly described later). Propagating planetary waves are apparent in the plot. Their speeds show some degree of variability: for instance, by eye it is possible to estimate that the negative anomaly around 75°E at the beginning of 1993 travels the whole longitude span (20°, corresponding to about 2000 km at this latitude) in about 450 days, resulting in a speed of about 5.1 cm/s, while the positive anomaly entering the plot from the east around April 1996 takes about 13 months to traverse the plot, giving a speed of about 5.9 cm/s. Figure 4b shows the 2D-FFT of the data shown in fig. 4a. The 2D-FFT has three main peaks, corresponding to signals that propagate in the plot with speeds between 5.5 and 6.4 cm/s. The peak marked as P3, with a wavelength of ~650 km and a period of ~133 days, corresponds to a first-mode baroclinic Rossby wave propagating at a speed of ~5.7 cm/s. This speed is slightly higher than the average speed of 4.7 cm/s predicted by the extended theory of Killworth et al. (1997) over the same area, indicated by the dashed red line. P3 and the four adjacent (but less prominent) peaks P4 to P7, having wavelengths

between  $\sim 1000$  and  $\sim 500$  km, and speeds between  $\sim 7.2$  and  $4.0$  cm/s, respectively, are components that can be most readily identified looking at the relatively smaller-scale, successive crests or troughs on the longitude/time plot itself. The other two major peaks, P1 (at the annual frequency) and P2 have longer wavelengths and periods but their speeds ( $6.4$  cm/s and  $5.5$  cm/s, respectively) are within  $\pm 15\%$  of the speed of P3, so it is not clear whether these may represent different propagation modes. In other cases, the peaks are at very different speeds from each other (such as the three signals at  $3$ ,  $1.9$  and  $0.9$  cm/s found at  $34^\circ\text{N}$  in the North Atlantic by Cipollini et al, 1997), and clearly indicate different modes of propagation. Figure 4b also shows the dispersion curve (1) from Rossby's linear theory (magenta line), computed with the average value of  $\lambda_1$  over the area, taken from Chelton et al. (1998), that is  $\lambda_1 = 42.9$  km; it can be noticed that all the peaks are above the curve, indicating that the speeds of the relevant components are faster than the linear theory ones, whereas there is much better agreement with the speed predicted by the extended theory of Killworth et al. (1997).

A major drawback of the 2D-FT method (and also of the RT, see below) is that in order to have distinct peaks in the spectrum, it must be applied to a portion of the data on a space and time sub-domain where the propagation characteristics do not vary too much. On the other hand, the resolution in the WF spectrum is inversely proportional to the width of the longitude and time intervals used. If the interval is too narrow, adjacent peaks will be indistinguishable from each other, so the selection of the sub-domain is a trade-off between resolution and homogeneity. Moreover the FFT is well suited for the study of waves which appear to be periodic in the space/time domain, and not appropriate for the study of single waves, such as the one observed by Jacobs et al. (1994) in the Pacific as a result of the 1982-83 El Niño.

## 2.2.2 Use of the Radon Transform

When the focus of the analysis is on the propagation speed rather than on the wavelength and period characteristics of the single components, the Radon Transform, first described by Radon (1917) and whose properties are described in Deans (1983), is more appropriate. The 2D-RT  $p(x', \phi)$  at a given angle  $\phi$  is the projection of an image (the longitude/time plot) along a direction normal to  $\phi$ :

$$p(x', \phi) = \int_{y'} f(x, y) \Big|_{\substack{x=x' \cos \phi - y' \sin \phi \\ y=x' \sin \phi + y' \cos \phi}} dy'$$

The RT of a longitude/time plot, computed for two different angles  $\phi_1$  and  $\phi_2$ , is shown in Figure 5. FT and RT are related by means of the *Projection-Slice theorem*:  $p(x', \phi)$  is equal to the inverse FT of a slice taken at the same angle  $\phi$  in the Fourier space. This is important as the lines at an angle  $\phi$ , both in the longitude-time space and in the WF space, are lines of constant speed, which can be readily computed from  $\phi$  by simple trigonometric considerations. Thus, computing the RT of the longitude-time plot for different values of  $\phi$ , and then its energy, is equivalent to computing the energy in the spectrum along lines of constant speed, and it is the most straightforward method to find the value of the speed for which that energy is maximum. In other words, it is a method that yields an objective estimate of the speed of the predominant propagating signal. To accomplish this, one needs to compute the RT energy (i.e., sum the squares of the RT) for every  $\phi$ , and find the value  $\phi_{\max}$  for which that energy is maximum (in figure 5 that angle is  $\phi_{\max} = \phi_1$ , which is orthogonal to the dominant direction of the alignments in the plot). The main propagation speed is then proportional to the tangent of  $\phi_{\max}$ . An application of the Radon Transform to find the speed of planetary wave propagation in longitude/time plots of sea surface temperature (SST) data from the Along-Track Scanning Radiometer (ATSR) on board the ERS-1 satellite has been described in detail by Hill et al., (2000). The fundamental steps in Hill et al.'s method, with some modifications, are described below, with reference to the longitude/time plot in figure 4a:

1. The longitude-time plot is pre-conditioned removing any outliers, filling any residual gaps (missing values due, for instance, to cloud coverage in SST data or to islands) with some form of interpolation and removing the mean of each row (fig. 4a includes this step already);
2. The window may then be filtered with a 2-D filter, for instance one designed to remove the high frequency noise or any variability at scales much smaller or much larger than those of Rossby waves. Different filter designs can be adopted, including local anomaly filters, various 'band-pass' filters to remove both very low frequency variability and the high frequency noise or a 'westward-only' filter like the one described in Cipollini et al., 2001, which highlights the westward propagating signals. A most selective version of the 'westward-only' filter, with unit response in the first

and third quadrants of the WF space (those being the westward-propagating components) and zero response in the 2<sup>nd</sup> and 4<sup>th</sup> quadrant in WF space (including the axes), has been used here to filter the longitude/time plot in figure 4a. This filter leaves the westward propagating signals untouched and completely rejects any stationary or eastward propagating one. The ‘westward-only’ filtered longitude-time plot is shown in figure 6a;

3. The Radon transform is performed for  $\phi$  varying from  $0^\circ$  to  $90^\circ$  in steps of  $1^\circ$ , and its energy or variance is computed for each  $\phi$ . The transform and its variance are shown in figures 6b and 6c, respectively;
4. The values of  $\phi$  in the local maxima of the standard deviation are orthogonal to the orientation of the alignments in the longitude-time plot, and thus can be converted into an objective measure of the speed of propagation. These maxima can be identified automatically, converted into propagation speeds and saved. A set of lines at an angle normal to  $\phi_{\max} = 46^\circ$ , that is normal to the angle of the large maximum in figure 6c, has been drawn over Figure 6a for reference (these lines correspond to a propagation speed of 5.6 cm/s). It is obvious that the broad peak in fig. 6c encompasses the planetary waves in the original longitude/time plot; its width is a measure of the spread in the speeds

Additional screening of the results is possible on the basis of the relative height of the peak in the RT standard deviation plot, as performed in the SST analysis by Hill et al. (2000), or on the basis of theoretical predictions as in the global example below.

The RT as described above can be easily automated and applied to longitude/time windows moving over the whole globe. Figure 7a shows the result of the 2D-RT analysis of subsets of merged T/P and ERS data of  $20^\circ$  longitude x 513 weeks centered at each integer latitude value and every  $2^\circ$  longitude in the oceans. For each 2D-RT the angle of maximum energy has been selected and the corresponding speed has been computed. The analysis has followed points 1 to 4 above, with the addition of further screening of the peaks on the basis of the speeds predicted by the extended theory by Killworth et al. (1997), recomputed using the newer climatologies in the World Ocean Atlas 1998 data (Antonov et al., 1998; Boyer et al., 1998), which are shown in figure 7b. When the speed of the maximum peak was less than 1/3 or more than 3 times the predicted theoretical speed in the same location, the second largest

peak has been selected instead, provided it passed the above criteria. Figure 7c shows the ratio of fig. 7a and 7b, for ease of comparison.

The agreement between satellite-derived speeds and Killworth et al's speeds is remarkably good at latitudes between  $15^\circ$  and  $35^\circ$  in both hemispheres (where both are significantly larger than those speeds estimated with the standard linear theory, as pointed out by Chelton and Schlax (1996) and Killworth et al. (1997)). This is true especially in the Atlantic and Indian Ocean, while in the Pacific, somewhat surprisingly, the observed speeds are almost everywhere slightly slower than the extended theory ones. Conversely, in a band at higher latitudes (approximately  $35^\circ\text{N}$  to  $40^\circ\text{N}$  in the North Atlantic,  $30^\circ\text{S}$  to  $40^\circ\text{S}$  in the Indian and South Atlantic and up to  $50^\circ\text{S}$  in part of the South Pacific, there are patches where the observed speeds can be up to 2-3 times larger than the extended theory ones. This is currently being investigated.

Within  $15^\circ$  of the equator, the satellite-derived speeds are lower than both the linear theory and the extended theory. There are two possible explanations for this:

1. The longitude span of  $20^\circ$  is too short to encompass the typical wavelengths of planetary waves close to the equator, resulting in aliasing of the wave characteristics (a variable size longitude span should then be used, with some complications in the processing).
2. In the tropics the 2D-RT preferentially picks up higher-order modes of propagation.

It is worth mentioning that the RT techniques just explained can be used for the study of eastward phenomena in longitude/time plots of data (using a different range of  $\phi$ ). It can also be extended to the three-dimensional case in order to study the directional properties of Rossby waves and estimate the meridional speed component in addition to the zonal one. A description of the three-dimensional extension of the RT is presented in Challenor et al. (2001). By applying this technique to T/P data in the North Atlantic, the same authors have verified that in most locations the dominant propagating signal is within  $\pm 10^\circ$  from pure westward.

## **3 Observations in other remotely-sensed datasets**

### ***3.1 Observations in SST data and their meaning***

As mentioned before, Hill et al. (2000) have found that the signature of planetary waves is almost ubiquitous in global fields of SST measurements by the ATSR instrument (referenced with respect to an *in situ* climatology). The SST-derived speeds computed by Hill et al agree very well with the predictions of the extended theory by Killworth et al. (1997), apart from some 'slower than theory' speeds at latitudes of 10-15° that might be due to the same reasons outlined for the T/P observations.

SST observations of planetary waves are very important. While the thermal signature of the waves may not be such a direct representation of their dynamical characteristics as is the SSH signal, it must be pointed out that it is the thermal signature which is influential for the processes of ocean-atmosphere interaction. The coupling between ocean and atmosphere can be, in turn, responsible for changes in the planetary wave characteristics, as hypothesized by White et al. (1998). In some cases simultaneous SST/SSH observations can provide additional information on the modal structure of the waves (as in Cipollini et al., 1997) or even, in conjunction with ocean colour data, on the mechanisms by which biology is affected by the waves; this will be discussed in §3.3.

It should be noted that a promising class of instruments for this kind of observations are passive microwave radiometers measuring SST. These measurements, whose relatively low geometrical resolution (tens of km) is still more than enough for the observation of large-scale phenomena, are unaffected by clouds and thus provide a good dataset to investigate planetary waves. Quartly et al. (2003) have found evidence of planetary waves in the Indian Ocean in data from the TMI on board TRMM and illustrate that with an example at 32°S. A similar example is presented in §3.3.

### ***3.2 Observations in ocean colour***

Recently, evidence of propagating signals with speeds consistent with those of planetary waves has been found in filtered longitude/time plots of phytoplankton chlorophyll concentration from ocean colour radiometers (Cipollini et al., 2001, Uz et al., 2001). Figure 8, taken from Cipollini et al., 2001, shows a longitude/time plot of OCTS and SeaWiFS data in

the Indian Ocean after high-pass and westward-only filtering (see the relevant paper for more details on the filters). A number of propagating anomalies are apparent in the plot. Their speed can be evaluated with the 2D-RT technique described in §2.2, giving a peak at 3.7 cm/s. By comparison, the same analysis on T/P data in the same location gives a peak at 4.0 cm/s, within 10% of the ocean-colour result. The ocean-colour-derived speeds observed by Cipollini et al. in various locations in the different ocean basins show a broad agreement with the other satellite observations and the extended theory.

A number of possible mechanisms may be responsible for the presence of the planetary wave signature in ocean colour data:

- i. Advection of chlorophyll gradients - advection of meridional gradients of phytoplankton due to the geostrophic currents associated with the passage of the waves. In this case phytoplankton acts just as a passive tracer;
- ii. Shoaling of the deep chlorophyll maximum - the modification of the isopycnals due to the passage of a wave could bring more phytoplankton cells closer to the surface or vice versa, and thus either affect the amount of phytoplankton seen by the satellite without changing its total (vertically-integrated) amount (see Charria et al., 2003), or increase/decrease growth, by bringing more cells into the euphotic zone or pushing them out of it.
- iii. Nutrient pumping effect - the modification in the upwelling of nutrients due to the raising and lowering of the thermocline associated with a wave, and thus a direct effect on the growth of a nutrient-limited population of cells. This is the so-called 'rototiller effect' (Siegel, 2001).

Understanding which mechanism predominates requires a careful intercomparison of the signature of the waves in different datasets, as explained below. The effect of planetary waves on biology could prove to be significant for studies of the global carbon cycle, especially if the occurrence of mechanism iii above is proved. Very recently, Killworth et al (2004) have carried out a global cross-spectral analysis of ocean colour and SSHA data and its comparison with theoretical predictions from models of the mechanisms listed above. Their main finding is that the horizontal advection of chlorophyll gradients is the main mechanisms over most of the ocean, although it cannot be ruled out that there exist locations where additional biological mechanisms (like mechanism iii above) may be responsible for at least part of the signal.

### ***3.3 Synergy of planetary wave observations in different datasets***

The following example illustrates how, by looking at the signature of the waves in different datasets, and in particular at their phase relationship, it is possible to infer more information about the underlying mechanisms of interaction between the waves and the SST and ocean colour fields. Figure 9 shows data at 32°S in the Indian Ocean from 4 different sensors flying on 4 different spacecraft: T/P SSHA, ocean colour data observed by SeaWiFS, SST from ATSR-2 and another SST field, but derived from TMI, the passive microwave sensor on the TRMM platform.

In figure 9 a spatial filter has been applied to each dataset in turn, to produce anomalies relative to the local mean. All four parameters display westward-propagating features. The signals are clearest in the SSH field, especially in the western half of the basin where the alignments of crests and troughs run parallel (i.e. with the same propagation speed) and each feature maintains approximately the same magnitude, albeit that the amplitude of separate features can vary from as little as 2 cm to more than 6 cm. The signals in the western basin have a wavelength of ~800 km, a period of ~7 months and a speed of ~4.4 cm/s. The chlorophyll signature of Rossby waves is by no means as clear as in SSH. There is a strong intra-annual variation; in the western half, the greatest proportional changes occurring around September 1998 (at the peak of the bloom), whereas in the east the chlorophyll anomalies are greatest in early 1999. However, within the limited extent of the time series it is not clear that this is a seasonal modulation.

In subplots c) and d) in fig. 9, which show the SST anomalies from infra-red and passive microwave sensors, it is very impressive just how well these two datasets agree — not just in the timing of propagation features but in their magnitude too. It should be recalled that these are two independent datasets using different technologies on different platforms. As the principal errors for infrared SST measurements are due to thin clouds and those for microwaves are due to wind speed and orientation, the retrieval errors for these two datasets are totally independent. Of the two, the waves appear clearer in the TMI data — thus proving the usefulness of TMI in monitoring large-scale features such as planetary waves. To ease the comparison of the features, four straight dashed lines are overlaid in the same location in all plots and have been positioned along some significant reductions in chlorophyll (Fig. 9b). The pair on the right clearly correspond to a much slower speed than those on the left, and might

indicate a higher-order propagation mode. Both of the slower features can be seen in the ATSR-2 data, with one clear and the other just discernible in the TMI values too.

When looking at the phase relationship of these different signatures it can be seen that all four lines demarking decreases in chlorophyll also lie close to local maxima in SST. However, the westernmost two (first baroclinic modes) delineate the change from below average SSH to above average i.e. the SSH signals lag the SST signature by approximately  $90^\circ$ , but lead the ocean colour signature by a similar amount. The bathymetry might play an important part, since there are significant ridges at  $97^\circ\text{E}$  and  $87^\circ\text{E}$ . In numerical models it has been noted that rapid changes in bathymetry can cause the interchange of energy between different baroclinic modes (Barnier, 1988).

In the southern hemisphere, the geostrophic velocities associated with the passage of a planetary wave crest are directed as shown in figure 10. If a parameter has a positive meridional gradient (shown schematically in fig. 10 as a front), which is the case for SST there, then the signal due to the resulting advection of this gradient should lead the SSH signal by approximately  $90^\circ$ , as shown in the bottom panel of figure 10. If, on the contrary, the meridional gradient is negative (this happens for phytoplankton at  $32^\circ\text{S}$ , where moving equatorwards there is a transition from the productive mid-latitude waters to the oligotrophic waters at the interior of the subtropical gyre), then the signal resulting from advection should trail the SSH signal by approximately  $90^\circ$ . This is what is observed for the data in figure 9. It can be concluded that, in this location of the Indian Ocean, lateral displacement due to advection is the predominant mechanism for the presence of an ocean colour and thermal signature of planetary waves. In the discussion above, and in the schematics in figure 10, it has been assumed that the advected tracer anomalies (chlorophyll or SST) decay and go back to equilibrium (their background values) in a much shorter time than the wave period, so that the displacement of the anomalies is approximately proportional to the instantaneous geostrophic velocity rather than to its integral; the ‘decay’ time of the advected parameter is, for instance, the time taken by SST to reach equilibrium with the overlaying atmosphere in virtue of heat exchange, or the mean life time of a population of phytoplankton cells. If the decay is comparable or longer than the wave period, the phase relationship changes, as discussed in detail by Killworth et al., 2004.

Quartly et al. (2003) show a case study at  $34^\circ\text{S}$  with similar results — chlorophyll decreases coinciding with temperature increases, slower speeds being apparent in the eastern basin, and

with no clear SSHA signal for the slower modes. North of about 30°S they note that the cross-correlation of temperature and chlorophyll anomalies is positive. This partially reflects the change in sign of the meridional chlorophyll gradient, however Quartly et al. (2003) note that between 25° and 30°S the gradient changes sign with the season, due to a strong secondary bloom of phytoplankton in February-March (Longhurst, 2001). This secondary bloom is only present for about half the years since 1997, covered by the SeaWiFS mission. Eddy activity along 25°-27°S may help mediate the development of this bloom (Srokosz et al., 2004) and could complicate the determination of the SSHA-chlorophyll phase relationship of planetary waves in this particular region.

Killworth et al. (2004) have examined the cross-correlation between SSH and chlorophyll concentration on a global basis, contrasting the observed phase relationship with that expected for the different mechanisms listed in section 3.2. For mid-latitudes (both southern and northern hemispheres) they show the phase difference between chlorophyll and SSHA signals agree well with the predictions of the advection mechanism, indicating that advection plays an important role. However there is less agreement on the amplitudes, the observed chlorophyll signal being often larger than what would be expected from pure horizontal advection. This could indicate the occurrence of vertical mechanisms, especially upwelling which in theory could give large chlorophyll signals in several regions of the world ocean and therefore could have an influence on primary production and the global carbon cycle. This marks the current frontier in planetary wave research.

## **4. Summary**

In 1897, Hough predicted the existence of long wavelength planetary waves, which correspond to north-south oscillations of the water column, but with the direction of propagation usually being close to due west. However, it was only in the 1990s that it was realised that they were prevalent in all ocean basins (up to a limiting turning latitude). The leap forward in observations, and consequently in theoretical studies, was due to the advent of long-term consistent global satellite datasets of a high quality. Planetary waves are usually most clearly seen in measurements of SSHA from spaceborne radar altimeters, despite the surface variation only being a few centimetres rather than the tens of metres variation deeper within the water column. A number of numerical techniques — Fourier Transform, Radon

Transform — can be used to derive the key parameters of the wave, viz. wavelength, period and speed. The latter is very important as it sets the response time of western boundary currents to disturbances that have occurred at the east of the ocean. The observed westward propagation speed is a few cm/sec (a few km/day) at mid-latitudes, and increases equatorward as predicted by theory. However, the speeds predicted by the original theory underestimated the true speeds by as much as a factor of two. Consequently there have been several revisions to the theory to include the effects of currents and sloping bathymetry.

The near-global observations of planetary waves in SST and ocean colour are an even more recent discovery, whose implications are not yet fully resolved. Assuming that SST and chlorophyll concentration vary with latitude, planetary waves would be expected to generate temperature and colour signatures through the simple north-south advection of water associated with the waves. Recent research has confirmed that this horizontal mechanism is certainly important, but some discrepancies between the observed and modelled signals, especially in the amplitude relationships between chlorophyll and SSHAs signals, may suggest that vertical mechanisms are at play in some regions. For instance, in some locations the meridional gradient in chlorophyll is minimal, so the horizontal advection mechanism could not explain the observed ocean colour signal in the first place, raising the prospect that planetary waves may actually be promoting plankton growth there. Quantifying the effects of planetary waves on the global carbon cycle, and the long-term variability of these effects, are some of the important questions now challenging scientists.

## References

- Antonov, J., Levitus, S., T. P. Boyer, M. Conkright, T. O'Brien, C. Stephens, 1998: *World Ocean Atlas 1998 Vols. 1-3: Temperature of the Atlantic/Pacific/Indian Ocean*. NOAA Atlas NESDIS 27. U.S. Gov. Printing Office, Wash., D.C., 166 pp.
- Barnier B., A numerical study on the influence of the Mid-Atlantic Ridge on nonlinear first-mode baroclinic Rossby waves generated by seasonal winds, *J. Phys. Oceanogr.*, *18*, 417-433, 1988.
- Boyer, T. P., Levitus, S., J. Antonov, M. Conkright, T. O'Brien, and C. Stephens, 1998: *World Ocean Atlas 1998 Vols. 4-6: Salinity of the Atlantic/Pacific/Indian Ocean*. NOAA Atlas NESDIS 30. U.S. Gov. Printing Office, Wash., D.C., 166 pp.
- Brigham, E. O., *The Fast Fourier Transform and its applications*, 448 pp., Prentice Hall, 1988.
- Challenor, P. G., P. Cipollini, D. Cromwell, Use of the 3-D Radon Transform to examine the properties of oceanic Rossby waves, *J. Atmosph. Ocean. Tech.*, vol. 18, no. 9, pp. 1558-1566, 2001. See also: Corrigendum, *J. Atmosph. Ocean. Tech.*, vol. 19, no. 5, p. 828, 2002.
- Charria, G., F. Mélin, I. Dadou, M.-H. Radenac, and V. Garçon, 2003: Rossby wave and ocean color: The cells uplifting hypothesis in the South Atlantic Subtropical Convergence Zone. *Geophys. Res. Lett.*, **30**, 10.129/2002GL016390.
- Chelton, D. B. and M. G. Schlax, Global observations of oceanic Rossby waves, *Science*, *272*, 234-238, 1996.
- Chelton, D. B., R. A. de Szoeke, M. G. Schlax, K. E. Naggar, and N. Siwertz, Geographical variability of the first baroclinic Rossby radius of deformation, *Journal of Physical Oceanography*, *28*, 433-460, 1998.

- Cipollini, P., D. Cromwell, M. S. Jones, G. D. Quartly and P. G. Challenor, Concurrent altimeter and infrared observations of Rossby wave propagation near 34° N in the Northeast Atlantic, *Geophysical Research Letters*,. 24 ,. 889-892, 1997.
- Cipollini, P., D. Cromwell, P. G. Challenor and S. Raffaglio, “Rossby waves detected in global ocean colour data”, *Geophysical Research Letters*,. 28 , 323-326, 2001.
- Deans, S.R., The Radon transform and some of its applications: John Wiley, 1983.
- Dewar, W. K., 1998: On “too fast” baroclinic planetary waves in the general circulation. *J. Phys. Oceanogr.*, **28**, 1739-1758.
- de Szoeke, R. A., and D. B. Chelton, 1999: The modification of long planetary waves by homogeneous potential vorticity layers. *J. Phys. Oceanogr.*, **29**, 500-511.
- Emery, W. and L. Magaard, Baroclinic Rossby waves as inferred from temperature fluctuation in the eastern Pacific, *Journal of Marine Research* **34**: 365-385, 1976.
- Fu, L.-L. and D. B. Chelton, Large Scale Ocean circulation, in *Satellite Altimetry and Earth sciences*, eds. L.-L. Fu and A. Cazenave, Academic Press, 2001.
- Fu, L.-L., Latitudinal and frequency characteristics of the westward propagation of largescale oceanic variability, submitted to *J. Phys. Oceanography*, 2004.
- Gill, A. E., *Atmosphere-Ocean Dynamics*, Academic Press, San Diego, 1982.
- Hill, K. L., I. S. Robinson and P. Cipollini, “Propagation characteristics of extratropical planetary waves observed in the ATSR global sea surface temperature record”, *Journal of Geophysical Research - Oceans*, v. 105(C9), pp. 21,927-21.945, 2000.
- Hough, S. On the application of harmonic analysis to the dynamical theory of the tides, Part I. On Laplace’s ‘oscillations of the first species’, and on the dynamics of ocean currents. *Philos. Trans. Roy. Soc., A*, **189**, 201-257, 1897.

- Jacobs, G. A., H. E. Hurlburt, J. C. Kindle, E. J. Metzger, J. L. Mitchell, W. J. Teague, and A. J. Wallcraft, Decade-scale trans-Pacific propagation and warming effects of an El Niño anomaly, *Nature*, **370**, 360-363, 1994.
- Jacobs, G. A., Born, G. H., Parke, M. E., and Allen, P. C., The global structure of the annual and semiannual sea surface height variability from Geosat altimeter data. *J. Geophys. Res.*, **97**, 17,813-17,828, 1992.
- Jacobs, G. A., W. J. Emery and G. H. Born, Rossby waves in the Pacific Ocean extracted from Geosat altimeter data, *J. Phys. Oceanogr.*, **23**, 1155-1175, 1993.
- Jain, A. K. , *Fundamentals of Digital Image Processing*, 569 pp., Prentice-Hall, 1989.
- Killworth, P. D., and Blundell, J. R., The effect of bottom topography on the speed of long extratropical planetary waves. *J. Phys. Oceanogr.*, **29**, 2689-2710, 1999.
- Killworth, P. D. and J. R. Blundell, 2003a: Long extra-tropical planetary wave propagation in the presence of slowly varying mean flow and bottom topography. I: the local problem. *J. Phys. Oceanogr.*, **33**, 784-801.
- Killworth, P. D. and J. R. Blundell, 2003b: Long extra-tropical planetary wave propagation in the presence of slowly varying mean flow and bottom topography. II: ray propagation and comparison with observations. *J. Phys. Oceanogr.*, **33**, 802-821.
- Killworth, P. D., D. B. Chelton and R. de Szoeke, The speed of observed and theoretical long extra-tropical planetary waves. *J. Phys. Oceanogr.*, **27**, 1946-1966, 1997.
- Killworth, P. D., P. Cipollini, B. M. Uz and J. R. Blundell, Physical and biological mechanisms for planetary waves observed in satellite-derived chlorophyll, *J. Geophys. Res.*, in press, 2004.
- Le Traon, P.-Y. and J.-F. Minster, Sea Level Variability and Semiannual Rossby Waves in the South Atlantic Subtropical Gyre, *J. Geophys. Res.*, **98**, 12,315-12,326, 1993.

- Liu, Z., 1999: Forced planetary wave response in a thermocline gyre. *J. Phys. Oceanogr.*, **29**, 1036-1055.
- Longhurst, A., A major seasonal phytoplankton bloom in the Madagascar Basin, *Deep Sea Research I*, 48, 2413-2422, 2001.
- McPhaden, M.J., The eleven-year El Niño?, *Nature*, **370**, 326, 1994.
- Nerem, R. S., Schrama, E. J., Kobalinsky, C. J., and Beckley, B. D., A preliminary evaluation of ocean topography from the TOPEX/POSEIDON mission. *J. Geophys. Res.*, 99, 24,565-24,583, 1994.
- Osychny, V. and P. Cornillon, Properties of Rossby Waves in the North Atlantic Estimated from Satellite Data, *J. Phys. Oceanography*, 34, 61-76, 2004.
- Parke, M.E., G. Born, R. Leben, C. McLaughlin and C. Tierney, Altimeter sampling characteristics using a single satellite, *J. Geophys. Res.*, 103, 10513-10526, 1998.
- Pedlosky, J., *Geophysical Fluid Dynamics*. 2nd Ed., Springer-Verlag, 710 pp., 1987.
- Polito, P. S., and P. Cornillon: Long baroclinic Rossby waves detected by TOPEX/POSEIDON. *J. Geophys. Res.*, 102, 3215– 3235, 1997.
- Polito, P. S., and W. T. Liu, Global characterization of Rossby waves at several spectral bands, *J. Geophys. Res.*, 108(C1), 3018, doi:10.1029/2000JC000607, 2003.
- Quartly, G. D., P. Cipollini, D. Cromwell and, P. G. Challenor, Rossby waves: Synergy in action, *Phil. Trans. Royal Society London A.*, 361 , 57-63, 2003.
- Radon, J., Über die Bestimmung von Funktionen durch ihre Integralwerte längs gewisser Mannigfaltigkeiten, *Berichte Sächsische Akademie der Wissenschaften. Leipzig, Math.–Phys. Kl.*, 69, 262-267, 1917. English translation in S.R. Deans, *The Radon transform and some of its applications*: John Wiley, pp. 204-217, 1983.
- Rossby, C. G., Planetary flow patterns in the atmosphere. *Q. J. Roy. Meteor. Soc.*, 66, 68-87, 1940.

- Rossby, C. G., and Collaborators, Relations between variations in the intensity of the zonal circulation of the atmosphere and the displacements of the semi-permanent centers of action. *J. Mar. Res.*, 2, 38-55, 1939.
- Siegel, D.A., The Rossby rototiller, *Nature*, v. 409, pp. 576-577, 2001.
- Srokosz, M. A., G. D., Quartly and J. J. H. Buck, A possible plankton wave in the Indian Ocean, submitted to *Geophysical Research Letters*, 2004.
- Subrahmanyam, B., I. S. Robinson, J. R. Blundell and P. G. Challenor, Rossby waves in the Indian Ocean from TOPEX/POSEIDON altimeter and model simulations, *Int. J. Remote Sensing*, 2001.
- Tokmakian, R. T. and P. G. Challenor, Observations in the Canary Basin and the Azores Frontal Region Using Geosat Data, *J. Geophys. Res.*, 98, 4761-4773, 1993.
- Uz, B. M., Yoder, J. A. & Osychny, V. Pumping of nutrients to ocean surface waters by the action of propagating planetary waves, *Nature* v. 409, pp. 597-600, 2001.
- Wang, L., and Koblinsky, C. J., Low-frequency variability in regions of the Kuroshio Extension and the Gulf Stream. *J. Geophys. Res.*, 100, 18,313-18,331, 1995.
- Wang, L., and Koblinsky, C. J., Low-frequency variability in the region of the Agulhas Retroflection. *J. Geophys. Res.*, 101, 3597-3614, 1996.
- White, W. B., "Annual forcing of baroclinic long waves in the tropical North Pacific Ocean." *Journal of Physical Oceanography* 7: 50-61, 1977.
- White, W. B., Tai, C.-T., and DiMento, J., Annual Rossby wave characteristics in the California Current region from the Geosat exact repeat mission. *J. Phys. Oceanogr.*, 20, 1297-1311, 1990.
- White, W. B., Chao, Y., and Tai, C.-K., Coupling of biennial oceanic Rossby waves with the overlying atmosphere in the Pacific basin. *J. Phys. Oceanogr.*, 28, 1236-1251, 1998.

## Figure Captions

Figure 1 – schematic of a first-mode baroclinic planetary wave in the northern hemisphere.

Figure 2 – (From Fu and Chelton, 2001). Upper panel: comparison between TOPEX/POSEIDON measured speeds (circles) and the zonal average of speed predicted from linear theory (solid line). Centre panel: ratio T/P-derived speeds vs linear theory. Lower panel: ratio T/P-derived speeds vs Killworth et al.'s extended theory. Solid circles are for locations in the Pacific, open circles for locations in the Atlantic and Indian (Note – copyright clearance needs to be sought for this figure)

Figure 3 – Schematic of the production of a longitude/time plot

Figure 4 – a) Longitude/time plot of merged T/P and ERS SSHAs (m) at 28°S in the Indian Ocean; b) Amplitude of the 2D-FFT of the longitude/time plot in a). The diagram has been flipped horizontally so that westward-propagating signals are on the left quadrant. Contours start from 100 m·degrees·days (dark blue contour) and increase in steps of 100 m·degrees·days. The approximate wavelength  $\lambda$ , period  $T$  and zonal speed  $c_x$  of the peaks are: P1 -  $\lambda \approx 2000$  km,  $T \approx 360$  days,  $c_x \approx 6.4$  cm/s; P2 -  $\lambda \approx 1000$  km,  $T \approx 211$  days,  $c_x \approx 5.5$  cm/s; P3 -  $\lambda \approx 650$  km,  $T \approx 133$  days,  $c_x \approx 5.7$  cm/s; P4 -  $\lambda \approx 1000$  km,  $T \approx 164$  days,  $c_x \approx 7.1$  cm/s; P5 -  $\lambda \approx 650$  km,  $T \approx 156$  days,  $c_x \approx 4.8$  cm/s; P6 -  $\lambda \approx 600$  km,  $T \approx 143$  days,  $c_x \approx 4.9$  cm/s; P7 -  $\lambda \approx 500$  km,  $T \approx 124$  days,  $c_x \approx 4.0$  cm/s. The magenta curve is eq. (1) with a Rossby radius of 42.9 km; the red dashed line corresponds to a speed of 4.7 cm/s which is the median speed from the extended theory of Killworth et al. (1997) over the area.

Figure 5 – Example of 2D Radon Transform of a longitude/time plot  $f(x,y)$  computed for two different angles  $\phi_1$  and  $\phi_2$

Figure 6 – a) same longitude/time plot as in Fig. 4, after westward-only filtering as described in the text. The superimposed solid lines have a slope corresponding to the speed of maximum energy in the RT, that is 5.6 cm/s. b) 2D-RT of the longitude/time plot and c) its standard deviation.

Figure 7 – a) Main zonal propagation speed from the 2D-RT analysis of longitude/time plots of merged **T/P and ERS SSHA**; b) zonal first-baroclinic mode speed from the extended

theory by Killworth et al. (1997), recomputed using the climatologies in the World Ocean Atlas 1998 data (Antonov et al., 1998; Boyer et al., 1998); c) ratio of a) to b).

Figure 8 – westward-propagating signals in a filtered longitude/time plot of Ocean colour (OCTS + SeaWiFS) data – from Cipollini et al., 2001.

Figure 9 – Longitude/time plots of four different datasets at 32°S in the Indian Ocean, filtered with a local anomaly filter. a) T/P SSHAs (m); b) chlorophyll concentration (expressed as ratio to local mean) from SeaWiFS; c) SST from ATSR-2 (°C); d) SST from TMI (°C); e) bathymetry.

Figure 10 – Mechanism of advection of meridional gradients by the geostrophic velocities associated with planetary waves. The arrows indicate the geostrophic velocities. Note that in the bottom panel it has been assumed that the ‘decay’ time of the advected parameter (for instance, the time taken by SST to reach equilibrium with the overlaying atmosphere in virtue of heat exchange, or the mean life time of a population of phytoplankton cells) is small with respect to the wave period, so that the displacement is approximately proportional to the instantaneous geostrophic velocity rather than to its integral (for more details on the effects of decay time see Killworth et al., 2004).

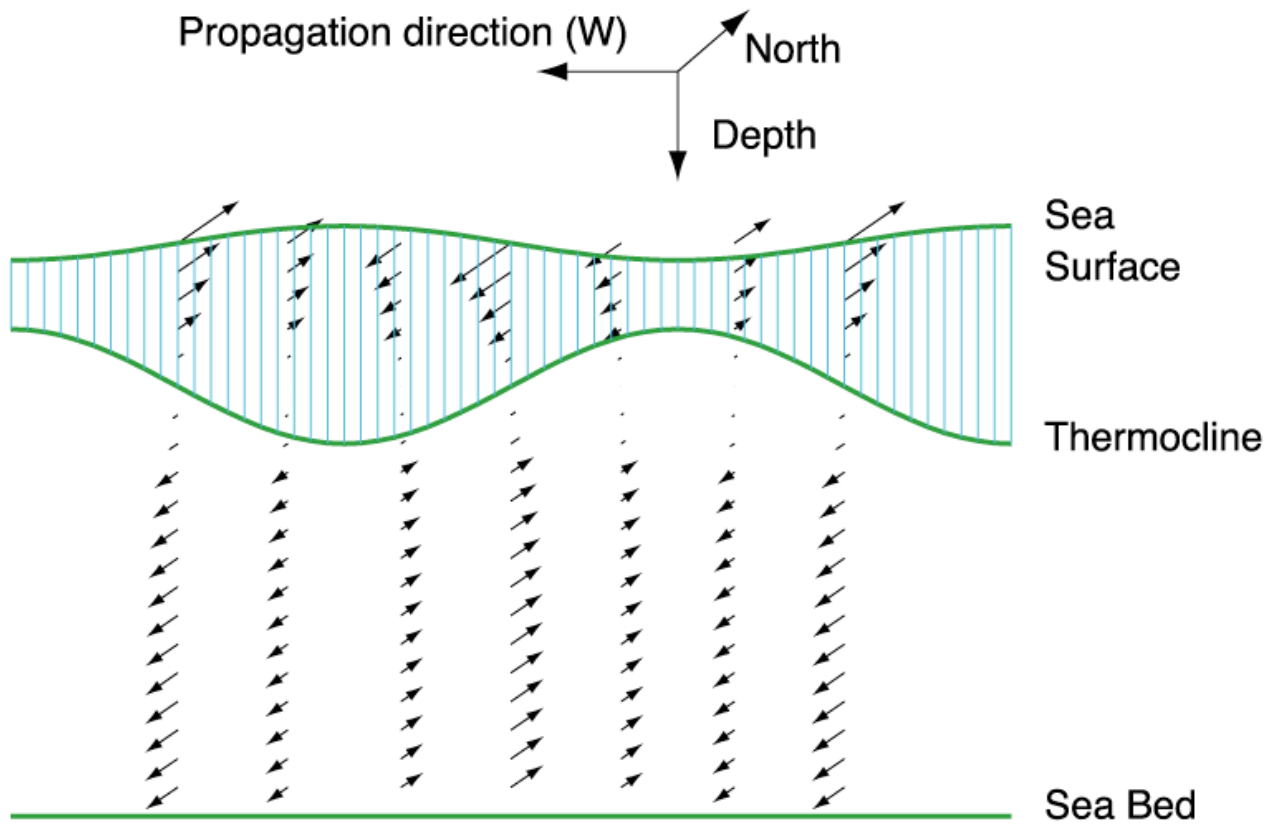


Figure 1

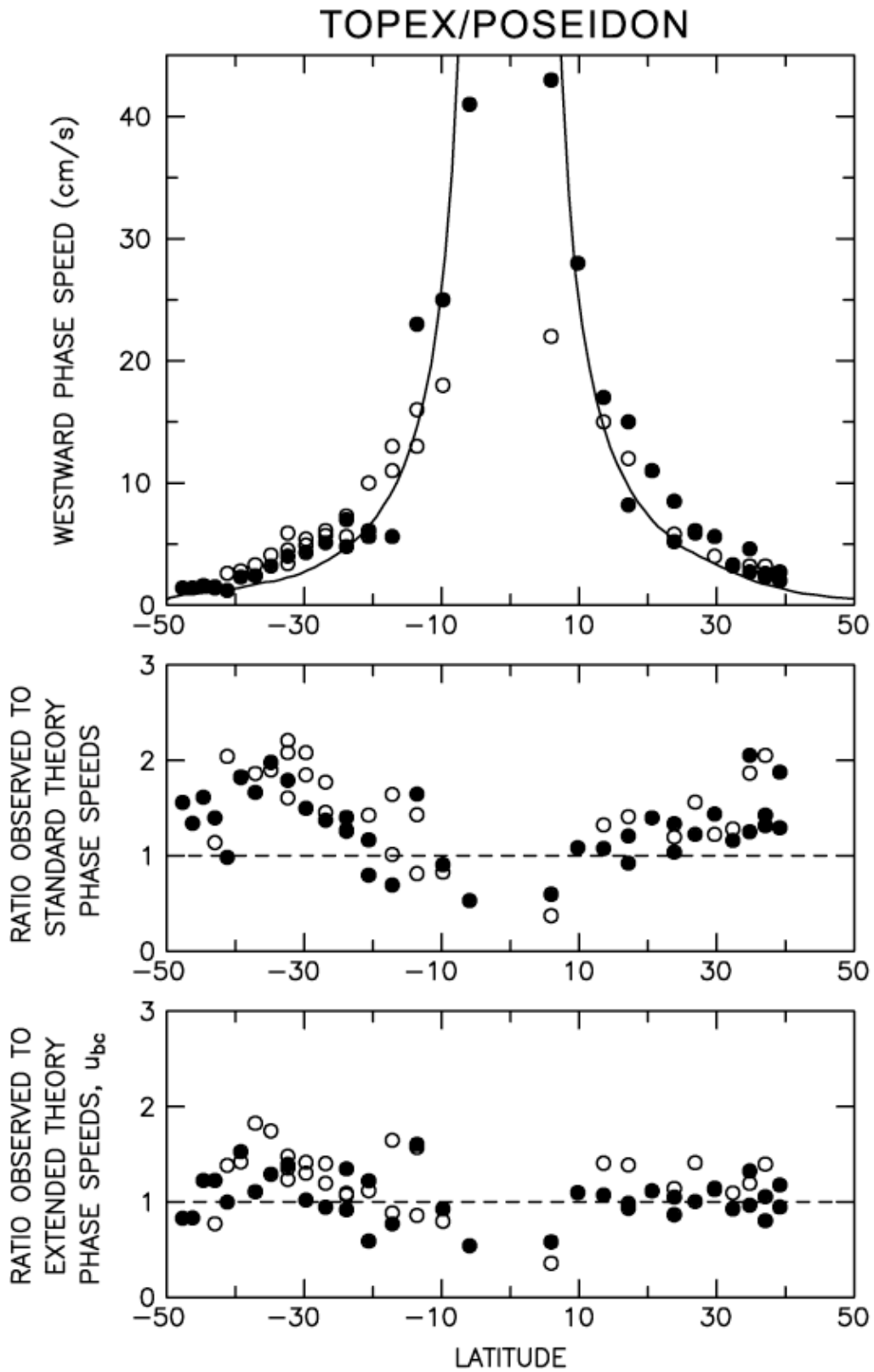
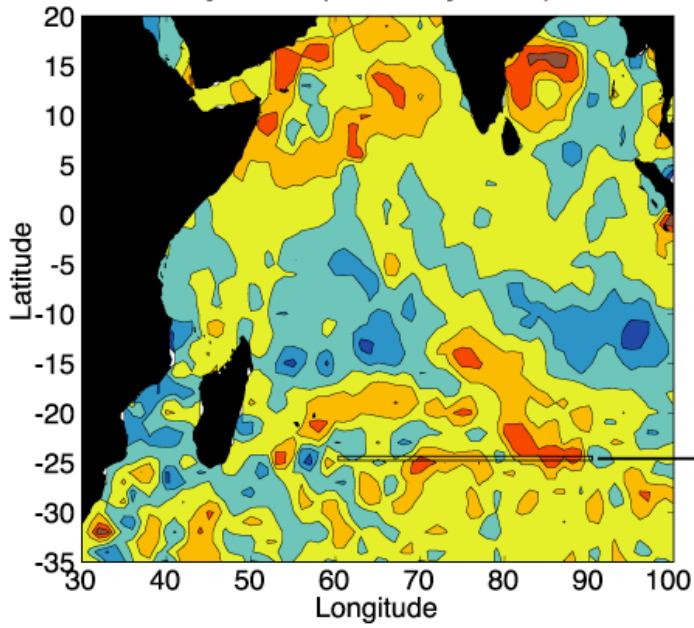


Figure 2

Sea Surface Height from TOPEX/POSEIDON  
cycle 60 (1-11 May 1994)



Hovmöller diagram at 25°S

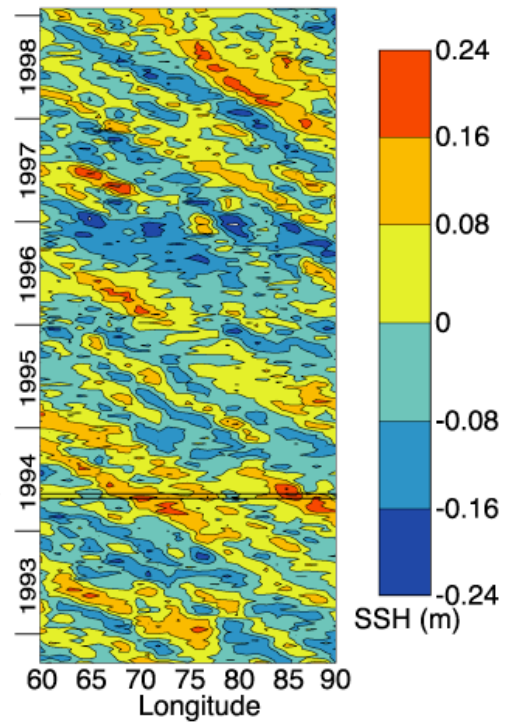


Figure 3

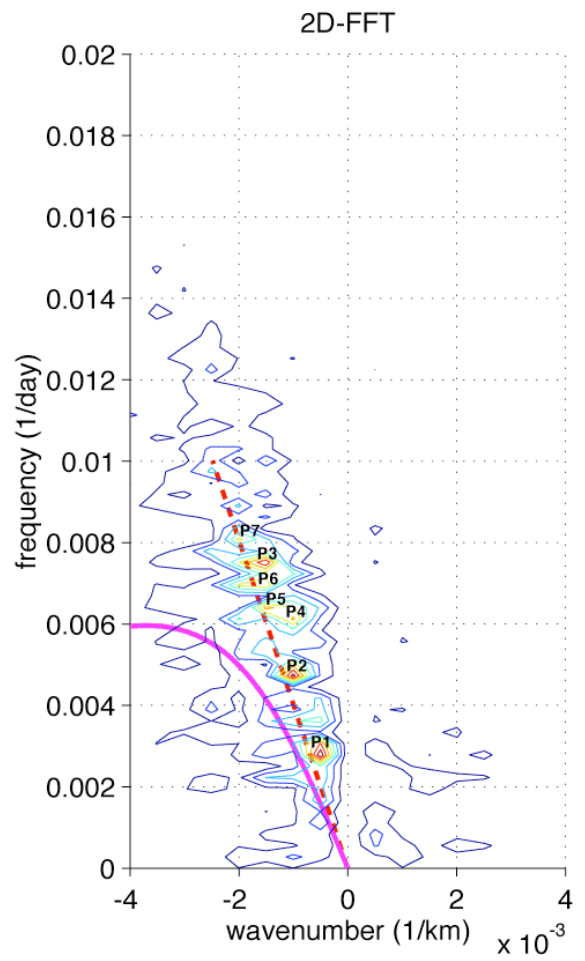
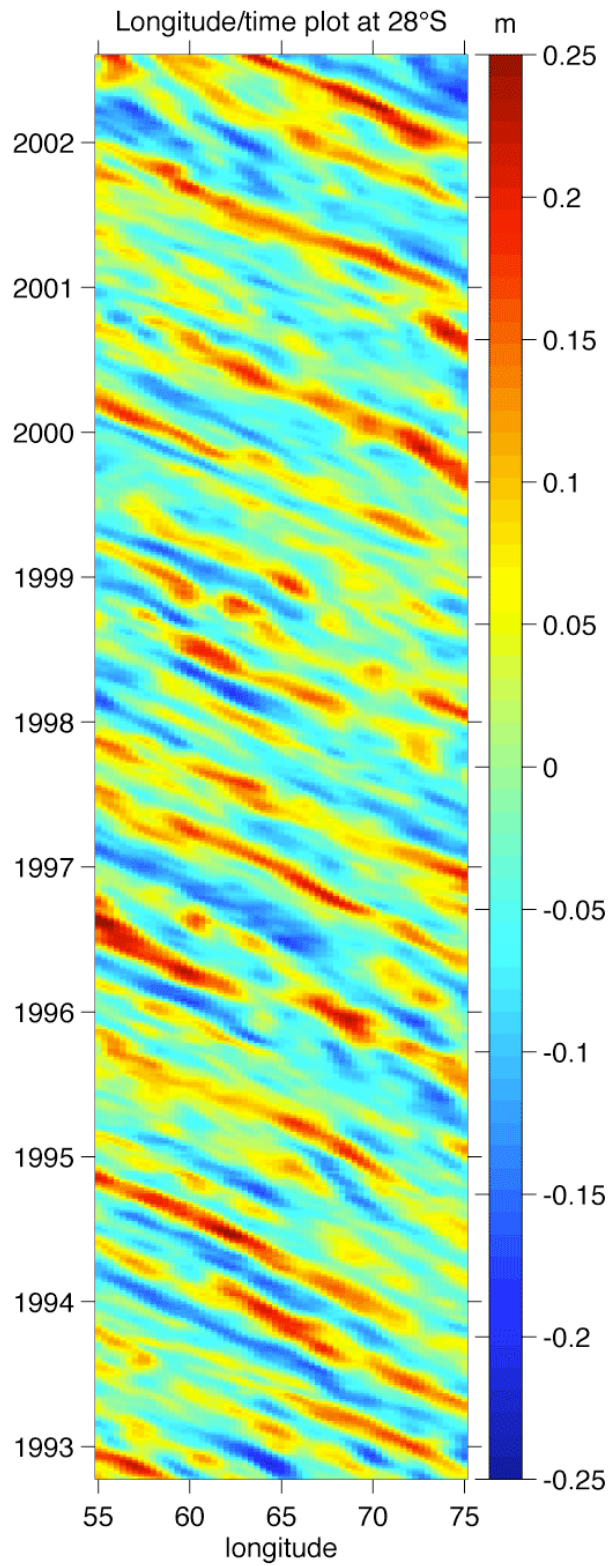
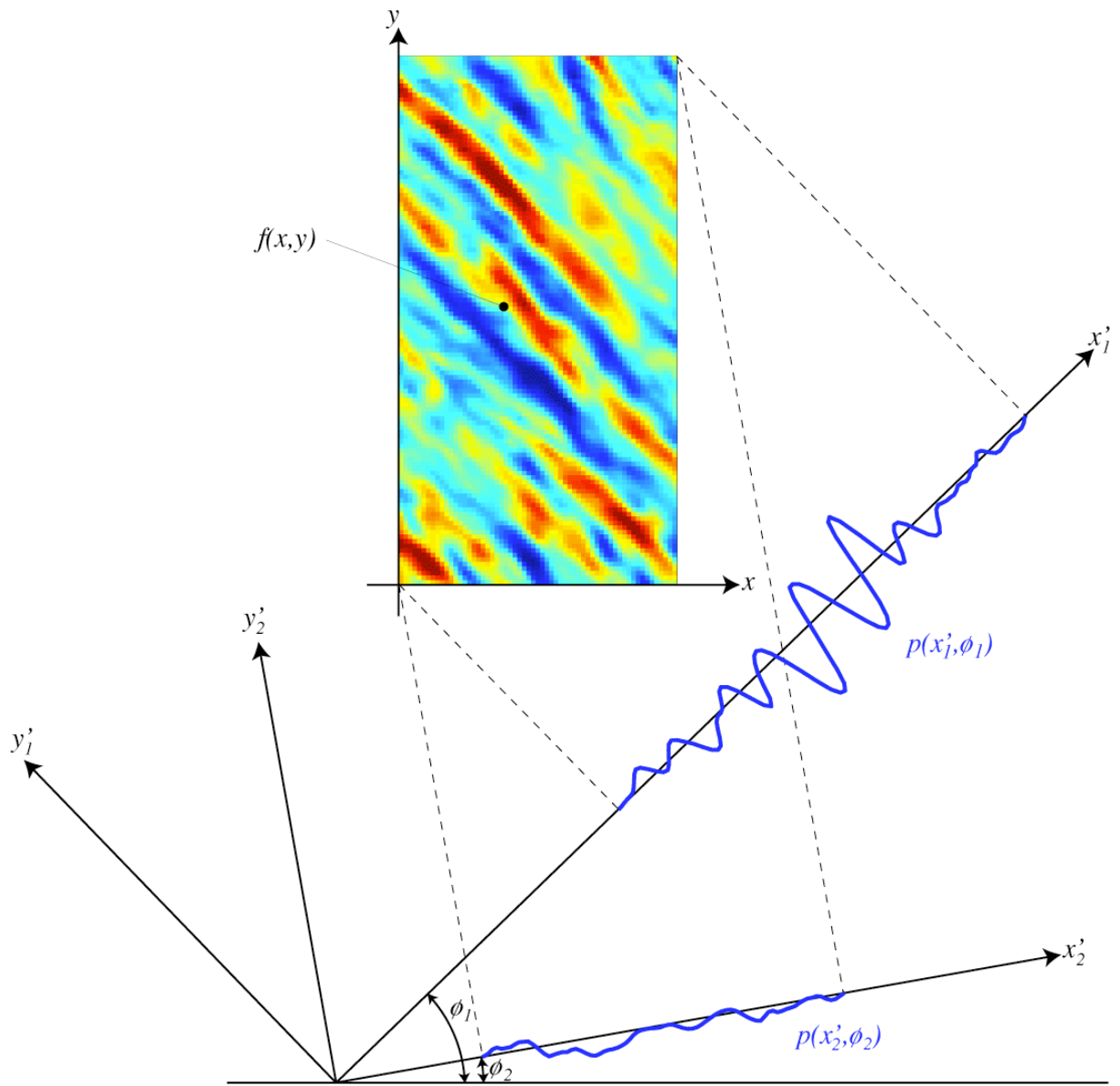
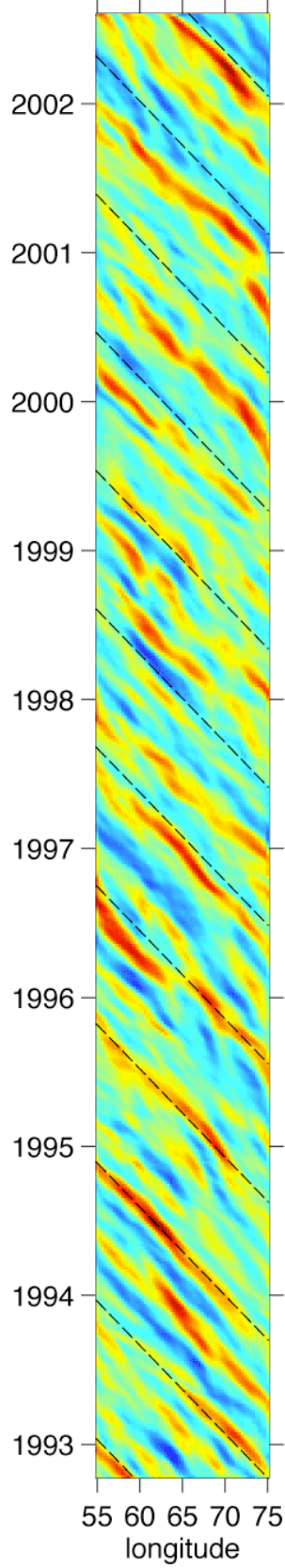


Figure 4

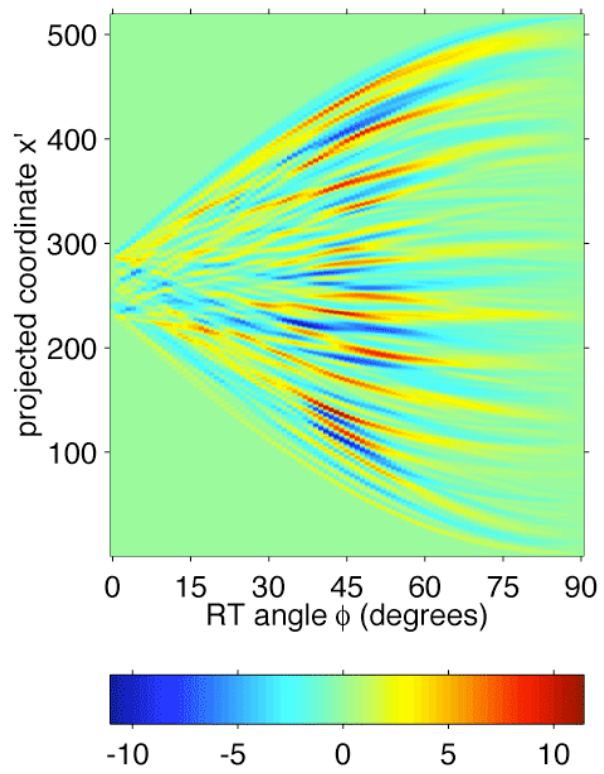


F i g u r e

Longitude/time plot at 28°S



2D-RT



Energy (variance) of 2D-RT

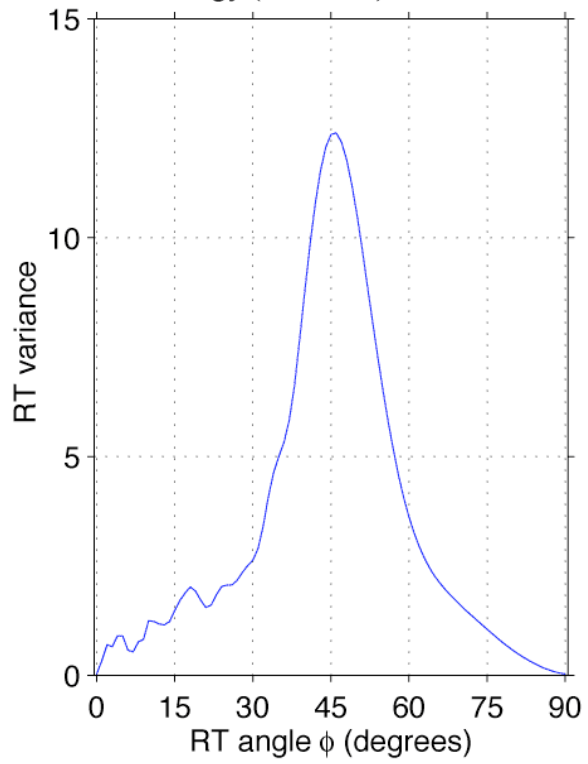


Figure 6

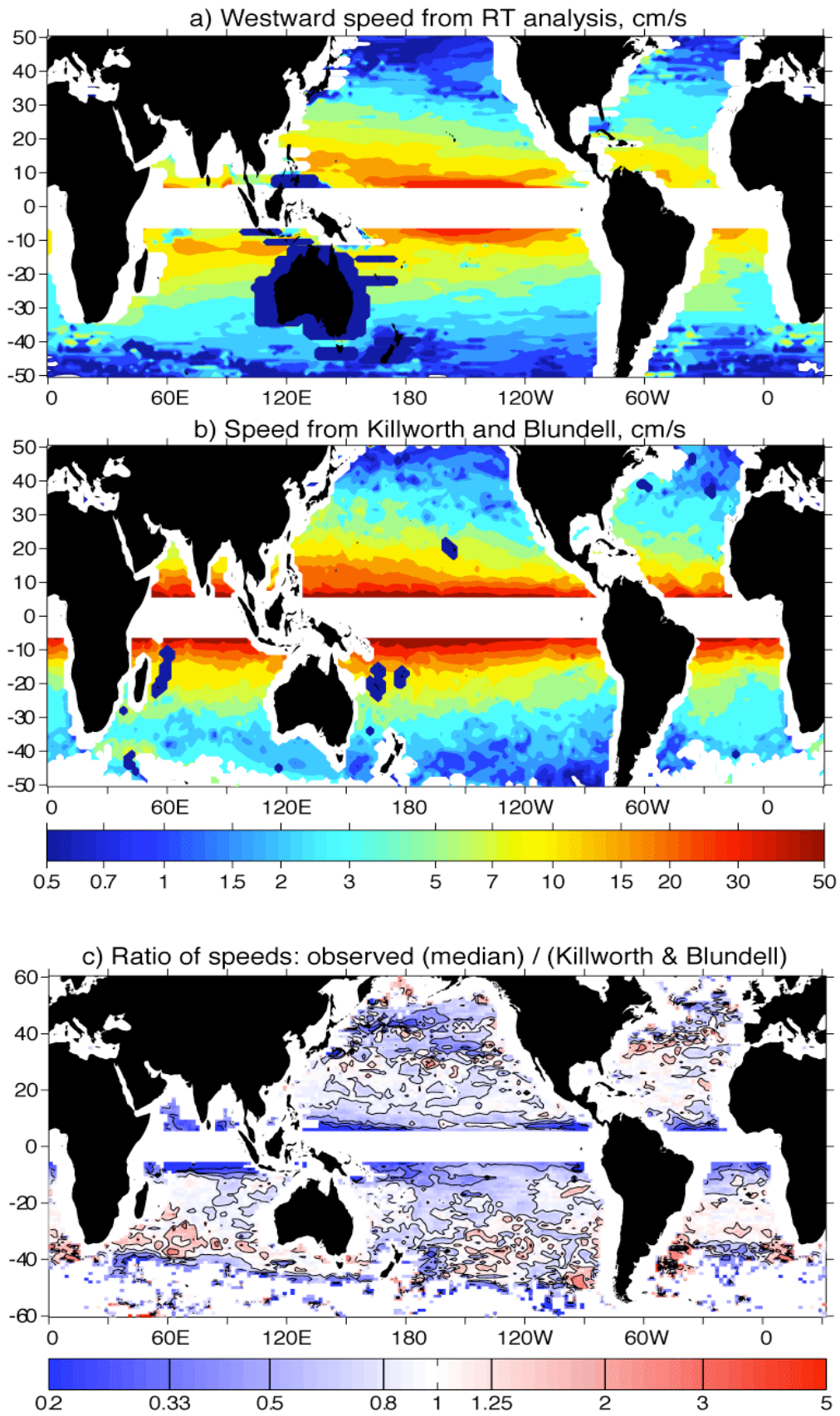


Figure 7

### Indian Ocean, 35.75°S

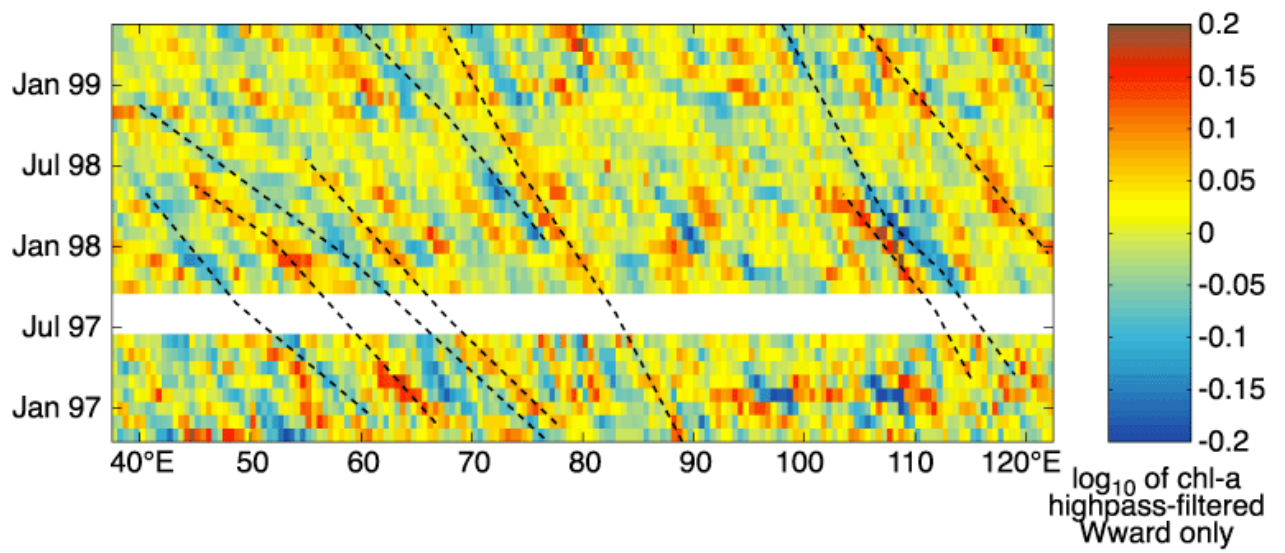


Figure 8

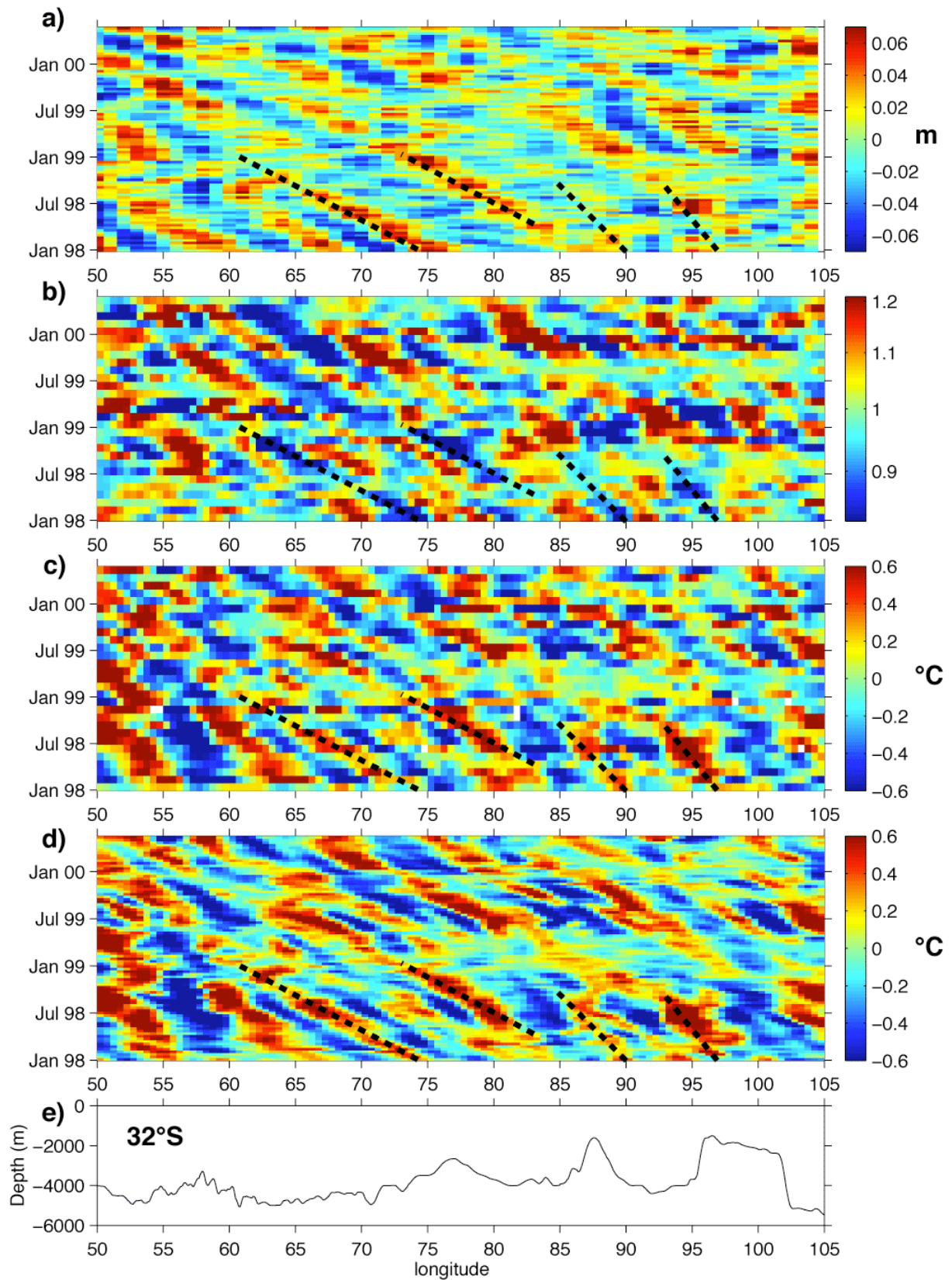


Figure 9

# Advection by geostrophic currents

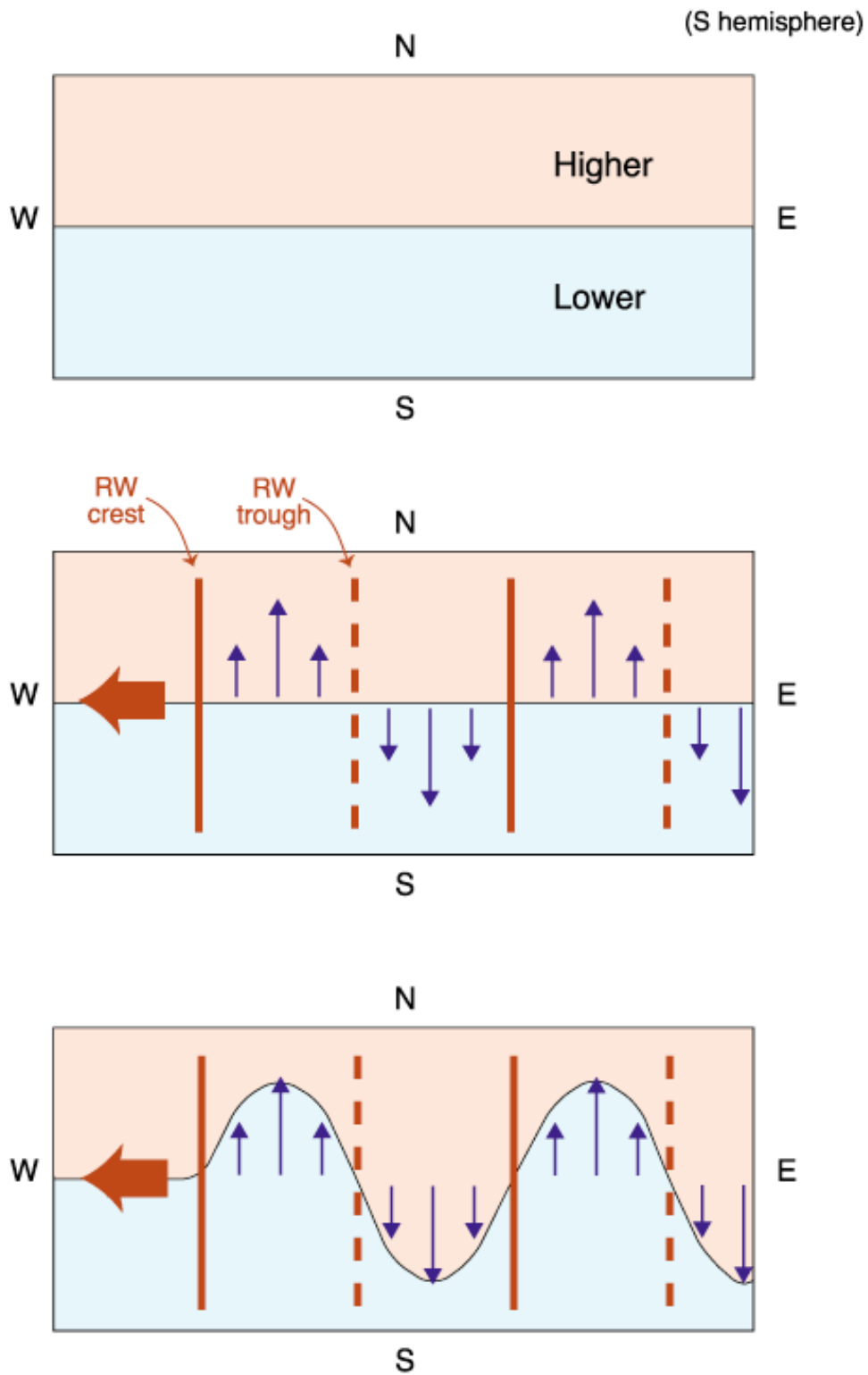


Figure 10